Available online at www.sciencedirect.com
ScienceDirect
Lithos 102 (2008) 25–42
LITHOS
www.elsevier.com/locate/lithos

Late Archean to Early Proterozoic lithospheric mantle beneath the western North China craton: Sr–Nd–Os isotopes of peridotite xenoliths from Yangyuan and Fansi

Yi-Gang Xu [a,*], J. Blusztajn [b], Jin-Long Ma [a], Katsuhiko Suzuki [c], J.-F. Liu [a], S.R. Hart [b]

[a] *Key Laboratory of Isotope Geochronology and Geochemistry, Guangzhou Institute of Geochemistry, Chinese Academy of Sciences, 510640 Guangzhou, China*
[b] *Woods Hole Oceanographic Institution, Woods Hole, Massachusetts, 02543, USA*
[c] *Institute for Research on Earth Evolution, Japan Agency for Marine-Earth Science and Technology, Natsushima, Yokosuka, 237-0061, Japan*

Received 17 October 2006; accepted 30 April 2007
Available online 8 May 2007

Abstract

Sr–Nd–Os isotopic analyses are presented for peridotite xenoliths from Tertiary alkali basalts in Yangyuan and Fansi with the aim of identifying and characterizing the relics of ancient lithospheric mantle that survived lithospheric removal in the western North China Craton (NCC). The analyzed samples are residual lherzolites and harzburgites, ranging from fertile to highly depleted (0.36–4.0 wt% Al_2O_3) composition. Some LREE-enriched samples are characterized by moderate $^{87}Sr/^{86}Sr$ (0.7044 to 0.7047) and low ε_{Nd} (−6.9 to −10.6), pointing to an EMI-type signature. This is distinct from the predominant depleted isotopic composition in mantle xenoliths from eastern China. Os isotopic ratios range from 0.1106 to 0.1325. The lower limit is the most unradiogenic value measured so far for Cenozoic basalt-borne xenoliths from eastern China. Two samples show radiogenic Os ratios higher than that of the primitive upper mantle, one sample has an anomalously high Os concentration (>9 ppb). These samples also show high La/Yb, consistent with the addition of radiogenic components during the infiltration of asthenosphere-derived and/or subduction-related melts in the lithospheric mantle. The remaining samples define positive correlations between $^{187}Os/^{188}Os$ and indices of melt extraction, which yield a model age of ~2.6 Ga. This age of melt extraction overlaps with the Nd model age of the overlying crust, indicating a coupled crust–mantle system in the western NCC. This contrasts with the decoupled nature in the eastern NCC, suggesting distinct mantle domains underneath the NCC. Such a heterogeneous age structure of the upper mantle is compatible with the view that the lithospheric removal was largely limited to the eastern NCC.
© 2007 Elsevier B.V. All rights reserved.

Keywords: Sr–Nd–Os isotopes; Peridotite xenolith; Lithospheric mantle; Age; Yangyuan and Fansi; Western North China Craton

1. Introduction

The North China Craton (NCC) experienced widespread lithospheric extension during the Late Mesozoic and Cenozoic, which resulted in the removal of a large portion (>100 km) of mantle lithosphere (Menzies et al.,

* Corresponding author. Tel.: +86 20 85290109; fax: +86 20 85290261.
E-mail address: yigangxu@gig.ac.cn (Y.-G. Xu).

0024-4937/$ - see front matter © 2007 Elsevier B.V. All rights reserved.
doi:10.1016/j.lithos.2007.04.005

1993; Griffin et al., 1998; Xu, 2001; Gao et al., 2002). This lithospheric thinning was accompanied by a change in mantle composition, probably due to the replacement of the thick, old, cold and refractory lithospheric keel by thin, young, hot and fertile mantle. In recent years, the timing, mechanisms and tectonic driving forces responsible for lithospheric removal have been intensely debated. For instance, two end-member models have been proposed as mechanisms of lithospheric thinning, i.e., delamination *versus* thermo-mechanical erosion. Different physical mechanisms involved in lithospheric thinning have distinct implications for the vertical extent of lithospheric removal (Reisberg et al., 2005). Delamination would probably result in the removal of the entire mantle lithosphere and part of the lower crust (Wu et al., 2003; Gao et al., 2004). Geophysical data indicate that the current lithospheric thickness beneath eastern China is 60–100 km; thus, the lithosphere may have been re-thickened by conductive cooling subsequent to the removal processes (Menzies and Xu, 1998; Xu, 2001). In this sense, the mantle lithosphere is young. In contrast, thermal erosion may remove only part of the mantle lithosphere, leading to the co-existence of old and young mantle lithosphere. If thermal erosion of the lithosphere induced by the upwelling of asthenosphere took place gradually from the base of the lithosphere, a stratified architecture is envisaged with the old lithospheric relict overlying the newly accreted one (Griffin et al., 1998; Menzies and Xu, 1998; Xu, 2001). If mantle upwelling preferentially focused along weak zones in the Archean lithospheric root (Yuan, 1996), dispersal of the ancient lithosphere in newly formed mantle will result.

The lateral extent of lithospheric thinning in the NCC is equally poorly constrained. The contrast in crustal and lithospheric thickness, topographic height and gravity anomaly across the Daxinganling-Taihangshan gravity lineament (DTGL, Fig. 1) suggests that lithospheric removal may be largely limited to the region east of the DTGL (Griffin et al., 1998; Menzies and Xu, 1998). Temporal and spatial evolution of Cenozoic volcanism further reveals that lithospheric thinning was probably diachronous with that in the western NCC being later than in the eastern NCC (Xu et al., 2004b). If thermo-mechanical erosion is the main mechanism of lithospheric thinning (Griffin et al., 1998; Xu, 2001; Xu et al., 2004a), and assuming that the lithospheric protolith under the NCC was entirely ancient prior to the Mesozoic, one can speculate that the present lithosphere mantle under the western NCC consists mostly of the relics of ancient mantle, in contrast to the co-existence of ancient mantle and newly accreted mantle in the eastern NCC. Clearly, the age of mantle samples from throughout the NCC will be needed to ultimately understand the nature of the thinning event.

The Re–Os isotopic system has proven useful in constraining the age of lithospheric mantle formation (Walker et al., 1989; Carlson and Irving, 1994; Pearson et al., 1995; Pearson, 1999; Reisberg and Lorand, 1995; Peslier et al., 2000a,b; Handler et al., 2003; Gao et al., 2002; Wu et al., 2003, 2006; Reisberg et al., 2005). This is because Os has a highly compatible nature and Re is incompatible during mantle melting. Therefore, depleted peridotites have high Os contents and low Re/Os ratios. Melting residue, if isolated in the lithosphere, will develop low time-integrated $^{187}Os/^{188}Os$ relative to the convective mantle. The Re–Os isotopic system was originally considered to be immune from disturbance due to metasomatic alteration because common mantle metasomatic agents (e.g., silicate and carbonatitic melt) are low in Os (Handler et al., 1997). Recent studies, however, have revealed a more complex response of the Re–Os system to metasomatic processes (Alard et al., 2002; Widom et al., 2003; Chesley et al., 2004; Griffin et al., 2004). A careful evaluation of the effect of metasomatism on the Re–Os system in peridotites is therefore necessary. When the effect of metasomatic sulfide addition is minimal, Re–Os isotope systematics remains a powerful tool to date the lithospheric mantle (Pearson et al., 2004).

In this study, analyses of major and trace element abundances and Sr–Nd–Os isotopic compositions have been carried out on a suite of peridotite xenoliths collected from Tertiary alkali basalts in Yangyuan (Hebei Province) and Fansi (Shanxi Province), western NCC. These data will be used to explore the effect of metasomatism on the composition of highly siderophile elements and to determine the age of the lithospheric mantle in the western NCC. Coupled with available data, the implications for the extent and nature of lithospheric removal in the NCC will be discussed.

2. Geologic background and petrographic characteristics

The NCC can be separated into two different tectonic domains by the N–S trend Daxinganling-Taihangshan gravity lineament (DTGL) (Ma, 1989; Menzies and Xu, 1998). The region located west to the DTGL is characterized by thick crust (>40 km), large negative Bouguer gravity anomalies, low heat

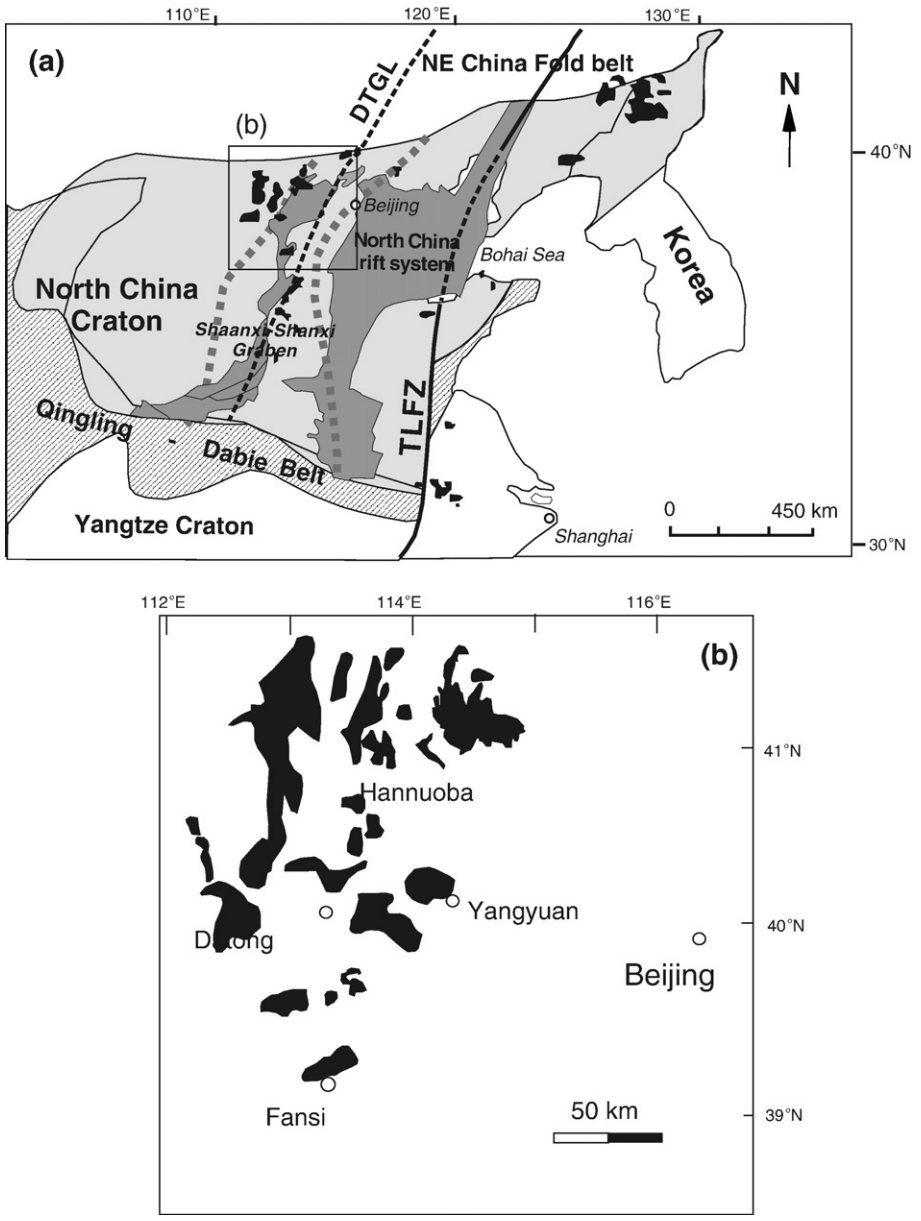

Fig. 1. (a) Simplified tectonic map of the North China Craton. Note that the North China Craton is cut by two major geological and geophysical linear zones—Tan-Lu fault zone (TLFZ) to the east and Daxinganling-Taihangshan gravity lineament (DTGL) to the west. Two shaded and dashed lines outline the Trans North China Orogen which separates western and eastern Blocks of the North China Craton (after Zhao et al., 2001). The Shaanxi-Shanxi rift system occurs in the Trans-North China Orogen. (b) Distribution of the Cenozoic basalts in the western North China Craton.

flow and a thick (>150 km) lithosphere (Fig. 1). In contrast, the crust beneath eastern NCC is thin (<35 km), the regional Bouguer gravity anomaly is weakly negative to positive, heat flow is high and lithosphere is inferred to be thin. Compilation of Sm–Nd isotopic data on crustal rocks led Wu et al. (2005) to argue that the crust was largely formed during the Early Proterozoic and Late Archean. It has been recently suggested that the DTGL was formed by diachronous lithospheric extension/thinning in the NCC, with that in eastern NCC taking place during the Late Mesozoic and that in western NCC during the Cenozoic (Xu, 2007).

Samples analyzed in this study were collected from alkali basalts at Yangyuan (western Hebei Province; 30–35 Ma; Liu et al., 1992) and Fansi (northern Shanxi

Province; 38–40 Ma). Both localities are situated adjacent to the northern part of the S-shape Cenozoic Shaanxi-Shanxi Rift system that extends from the southern margin of the Loess Plateau north-northeastward across the plateau (Fig. 1). Oligocene to Quaternary basalts are distributed in this region. The xenoliths from Yangyuan are large and fresh with maximum diameters of over 50 cm. The dominant xenoliths are spinel peridotites with subordinate pyroxenites. Xenoliths from Fanshi are generally small (mostly ~1–5 cm) and are loose. Pyroxenites are rare in this locality.

Peridotites from this region are similar to Group I peridotites (Frey and Prinz, 1978) with textural variation from protogranular to porphyroclastic (Mercier and Nicolas, 1975). Both lherzolite and harzburgite are present (Fig. 2a). The typical mineral assemblage is olivine (ol, 50–81%), orthopyroxene (opx, 20–34%), clinopyroxene (cpx, 1.4–16.7%) and spinel (sp, 0.8–3.8%). Volatile-bearing accessory minerals such as amphibole and carbonate are not observed. In a plot of modal olivine *versus* Fo (Fig. 2b), most samples plot in the Phanerozoic and Proterozoic domains, with only a few samples located marginally within the Archean field.

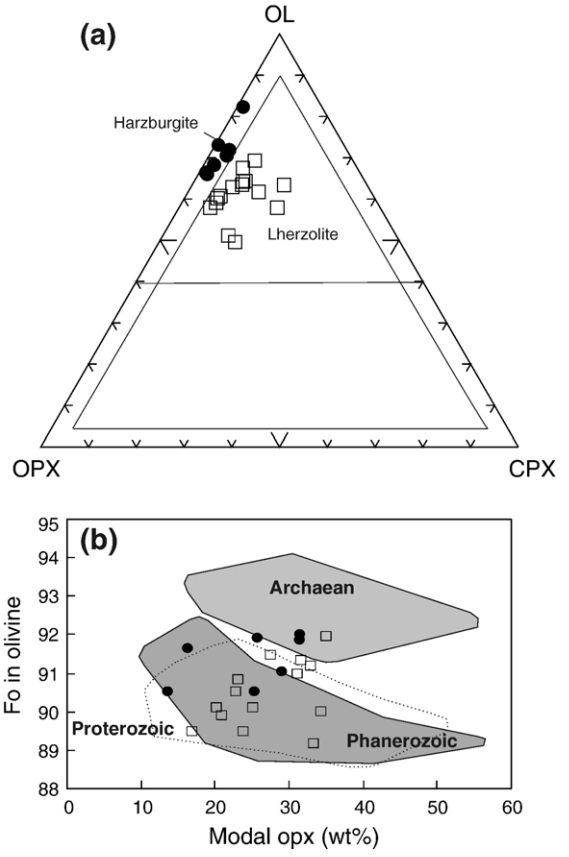

Fig. 2. (a) Modal composition of the peridotite xenoliths from Yangyuan and Fansi. (b) Modal orthopyroxene *versus* forsterite content in olivine. Complied fields for xenoliths found in Archean, Proterozoic and Phanerozoic crust are from Menzies (1990).

3. Analytical methods

Major and trace element compositions were determined using an X-ray fluorescence spectrometer (XRF) and inductively coupled plasma-mass spectrometry (ICP-MS), respectively, at the Guangzhou Institute of Geochemistry, Chinese Academy of Sciences (GIGCAS). Analytical procedures are described by Goto and Tatsumi (1996) and Xu (2002). For Sr–Nd isotopic analyses, cpx separates (~50 mg) of a subset of samples were dissolved in distilled HF-HNO_3 Savillex screwtop Teflon beakers at 150 °C overnight. Sr and REE were separated on columns made of Sr and REE resins of the Eichrom Company using 0.1% HNO_3 as elutant. Separation of Nd from the REE fractions was carried out on HDEHP columns with a 0.18N HCl elutant. The isotopic analyses were performed using a Micromass Isoprobe Multi-Collector ICPMS at GIGCAS. Measured Sr and Nd isotopic ratios were normalized using a $^{86}Sr/^{88}Sr$ value of 0.1194 and a $^{146}Nd/^{144}Nd$ value of 0.7219, respectively. The Sr and Nd blanks during the period of analyses were 0.5 ng and 0.3 ng, respectively. Analyses of standards during the period of analysis are as follows: NBS987 gave $^{87}Sr/^{86}Sr = 0.710243 \pm 14$ (2σ); Shin Etou gave $^{143}Nd/^{144}Nd = 0.512124 \pm 11$ (2σ), equivalent to a value of 0.511860 for the La Jolla international standard (Tanaka et al., 2000).

Osmium concentration and isotopic ratios were measured at Woods Hole Oceanographic Institution (WHOI) following the techniques described by Hassler et al. (2000). Powdered whole rock samples (about 1.5 g) were spiked with an in-house mixed spike enriched in ^{190}Os. The sample and spike mixtures were mechanically mixed in a ceramic crucible and were then combined with a ~5 g of flux consisting of sulfur, nickel and Na-borate with 1:2:15 proportions. Whole rock crucibles were fused at 1000 °C for 1.5 h. The NiS beads from the whole rocks were dissolved in 6.2 N HCl at ~150 °C and filtered through a 0.45-μm cellulose filter. The filter paper was then dissolved in 1 ml concentrated HNO_3, in a Teflon screw-cap beaker on hot plate at 100 °C for 45 min before sparging, during which oxidation of Os to OsO_4 was achieved. The acid solution was then

diluted ~5-fold with ultrapure water and a screw cap with inflow and outflow tubes was placed on the breaker. This cap allowed argon to bubble through the solution, via perforated tubing, thereby carrying the volatile OsO_4 into the torch for analyses (Hassler et al., 2000). Measurement of Os composition and concentration was carried out on a Finnigan Element 2 ICP-MS with argon flow rates being adjusted to around 1.35 L/min. Each analysis consisted of 30 runs. During the course of this study the whole chemistry Os blank was about 0.93 pg/g with $^{187}Os/^{188}Os$ of 0.64. In-run 2 sigma precision for $^{187}Os/^{188}Os$ measurement was about 0.5–1%. Repeated analyses of 1.25 ng and 400 pg in-house Os standard solution yielded an average $^{187}Os/^{188}Os = 0.17399 \pm 0.29\%$ and $^{187}Os/^{188}Os = 0.17432 \pm 0.55\%$, respectively.

4. Results

4.1. Major and trace elements

Whole rock geochemical data are listed in Table 1 and a brief summary is presented here. Al_2O_3 and CaO are negatively correlated with MgO (Fig. 3). The most fertile lherzolite sample (e.g., FS-1) is compositionally similar to the primitive mantle (Jagoutz et al., 1979; Hart and Zindler, 1986). Specifically, harzburgites have higher MgO contents and lower Al_2O_3 and CaO contents than lherzolites indicating a higher degree of partial melting for the harzburgites (Table 1; Fig. 3). The MgO content of the most refractory sample (YG-19) is 50%. Al_2O_3 and CaO contents in this sample are down to 0.36% and 0.12%, respectively.

Similar compositional distinction between lherzolites and harzburgites is also reflected in mineral chemistry (Table 2). For example, Cr# values of spinel (0.096–0.22) in lherzolites are lower than those in harzburgites (0.23–0.58). As $Cr\#_{Sp}$ is positively proportional to the degrees of partial melting, this implies that harzburgites underwent a higher degrees of melt extraction compared with lherzolites. Equilibrium temperatures for the Yangyuan peridotites, estimated using Ca-in-Opx thermobarometer of Brey and Kohler (1990), range from 916 °C to 1050 °C (Table 2). No difference in equilibrium temperature is observed between harzburgites and lherzolites.

The Yangyuan and Fansi peridotites exhibit substantial variations in both absolute concentration of trace elements (Table 1) and chondrite-normalized REE patterns. Three REE patterns for Cpx separates can be distinguished (Fig. 4). The first type is characterized by a flat HREE $[(Ho/Yb)_n = 1.03–1.15]$ pattern and a LREE-depleted pattern $[(La/Yb)_n = 0.34–0.58]$. Primitive mantle-normalized element abundances gradually decrease from MREE to Rb forming a smooth trend line. This pattern shows a pronounced negative Ti anomaly but no Nb and Ta anomalies (Fig. 4a, b). The second type pattern is characterized by relatively flat REE pattern (Fig. 3c). YYB-5 and YYB-7 possess a weak HREE fractionation with the apex at Nd. YYB-8 exhibits a weak LREE-enrichment. These samples exhibit negative Zr, Hf and Ti anomalies but no Nb and Ta anomalies (Fig. 3d). The third type pattern is characterized by LREE enrichment $[(La/Yb)_n = 2.7–110]$ and pronounced negative HFSE anomalies (Fig. 4e, f).

4.2. Sr–Nd isotope

$^{87}Sr/^{86}Sr$ ratio of Cpx in the Yangyuan peridotites ranges from 0.7031 to 0.7047. $^{143}Nd/^{144}Nd$ ratios have a wide variation from 0.5121 to 0.5136 (Table 2). These isotopic compositions are distinctly different from that of the host basalts (Fig. 5a). ε_{Nd} values of the LREE-enriched samples YYB-3 and YYB-9 are −10.6 and −6.9, respectively. However, their $^{87}Sr/^{86}Sr$ ratios are only moderately enriched (0.7044–0.7047). This may indicate a contribution from an EMI-type component (Fig. 5a). Although YYB-1 is also LREE enriched, it has a positive ε_{Nd} value and plots well within the Nd isotopic range of the LREE-depleted samples ($\varepsilon_{Nd} = +5$ to +8). The ε_{Nd} values of the samples with the second type of REE pattern ($\varepsilon_{Nd} = 1.2$) are between those of the LREE-depleted and the LREE-enriched samples. Nd model ages range from future ages to older than that of the Earth (Table 2). However, most of LREE-depleted samples have Nd model ages between 2.0 and 2.8 Ga.

4.3. Os concentration and isotopic composition

Osmium concentrations in all but one sample range between 0.3 ppb and 2.8 ppb (Table 2; Fig. 6). These Os concentrations are similar to off-cratonic spinel peridotites from around the world (Handler et al., 1997; Meisel et al., 2001; Peslier et al., 2000a; Pearson et al., 2004; Reisberg et al., 2005) but are lower than Os concentrations in peridotite massifs. The most refractory sample YG-19 is characterized by anomalously high Os content (9 ppb). No clear correlation is found between $^{187}Os/^{188}Os$ and Os and La/Yb for the whole suite (Fig. 6a, b).

Whole rock $^{187}Os/^{188}Os$ isotopic compositions measured by ICP-MS at WHOI range from 0.1106 and

Table 1
Major and trace element composition of whole rock peridotites from Yangyuna and Fansi

	Yangyuan										
	YYB-1	YYB-2	YYB-3	YYB-4	YYB-5	YYB-6	YYB-7	YYB-8	YYB-9	YYB-10	YG-1
SiO_2	44.00	46.07	46.40	46.73	45.46	45.66	44.91	46.05	46.33	45.32	44.69
TiO_2	0.01	0.02	0.03	0.06	0.02	0.08	0.01	0.06	0.01	0.05	0.09
Al_2O_3	0.63	1.45	2.10	2.15	1.33	2.70	0.89	2.37	0.72	2.22	2.61
Fe_2O_3	9.73	9.03	8.89	8.85	9.80	9.28	9.75	9.16	8.86	8.96	9.09
MgO	45.79	42.75	40.84	40.55	42.89	40.07	44.74	40.55	43.54	40.29	40.62
MnO	0.12	0.12	0.12	0.12	0.13	0.12	0.12	0.12	0.12	0.12	0.13
CaO	0.47	0.90	1.98	1.85	0.86	2.00	0.44	1.91	0.79	2.17	2.20
Na_2O	0.04	0.07	0.12	0.17	0.06	0.20	0.04	0.21	0.03	0.11	0.06
P_2O_5	0.01	0.01	0.01	0.01	0.01	0.01	0.00	0.01	0.01	0.01	0.01
K_2O	0.01	0.00	0.02	0.03	0.02	0.02	0.00	0.03	0.02	0.03	0.01
LOI	−0.87	−0.49	−0.73	−0.48	−0.63	−0.39	−0.88	−0.71	−0.49	0.50	0.17
Total	99.94	99.94	99.77	100.04	99.94	99.76	100.03	99.77	99.94	99.77	99.68
Mg#	0.90	0.90	0.90	0.90	0.89	0.89	0.90	0.89	0.90	0.90	0.90
Sc	5.08	7.80	11.98	10.54	6.52	11.02	5.47	10.45	7.85	9.00	11.40
Ti	40.8	125.4	186.5	338.4	126.6	453.6	63.4	374.8	43.6	267.0	368.0
V	21.88	31.02	48.04	44.96	26.72	48.44	21.62	45.22	26.56	39.80	42.30
Cr	3171	2224	2338	2259	1969	2116	2005	2210	1505	1967	2163
Mn	961.2	939.2	966.8	956.0	969.4	971.0	958.2	968.4	944.8	965.2	937.0
Co	122.3	103.4	106.0	103.5	108.6	100.7	113.2	101.4	105.1	100.9	101.0
Ni	2424	2070	2095	2071	2129	1929	2309	2016	2164	1977	2396
Cu	14.88	8.82	17.68	17.94	11.35	15.21	8.66	17.11	9.00	12.35	16.10
Zn	32.28	29.50	32.84	30.66	30.00	32.16	34.70	30.34	26.96	28.54	38.50
Ga	1.03	1.52	1.95	1.95	1.50	2.42	1.03	2.06	0.69	1.77	2.05
Ge	0.89	0.88	1.01	0.95	0.89	0.97	0.82	0.95	0.94	0.91	0.71
Rb	1.67	0.80	1.70	1.31	0.88	0.78	0.46	1.11	1.93	3.47	1.52
Sr	9.99	6.34	16.30	18.56	9.55	16.68	3.49	28.48	12.76	23.68	13.19
Y	0.13	0.43	1.55	1.50	0.46	2.08	0.24	1.85	0.12	1.20	1.69
Zr	5.20	4.52	6.87	6.62	3.57	6.77	2.45	6.17	2.78	3.40	3.11
Nb	0.19	0.12	0.30	0.43	0.16	0.27	0.07	0.57	0.96	0.15	0.49
Ba	1.51	0.02	3.24	7.36	1.04	2.97	1.61	2.83	3.39	2.02	3.73
La	0.183	0.055	0.625	0.320	0.109	0.264	0.026	0.516	0.725	0.068	0.230
Ce	0.445	0.142	1.743	0.758	0.252	0.646	0.064	1.014	0.763	0.166	0.560
Pr	0.051	0.019	0.251	0.107	0.036	0.097	0.009	0.131	0.061	0.028	0.080
Nd	0.211	0.097	0.991	0.498	0.151	0.497	0.040	0.579	0.201	0.167	0.420
Sm	0.049	0.034	0.189	0.149	0.044	0.167	0.014	0.175	0.034	0.069	0.120
Eu	0.013	0.012	0.056	0.057	0.015	0.064	0.006	0.068	0.009	0.030	0.050
Gd	0.037	0.044	0.168	0.196	0.055	0.251	0.021	0.242	0.027	0.121	0.200
Tb	0.006	0.008	0.031	0.035	0.009	0.047	0.004	0.042	0.004	0.026	0.040
Dy	0.029	0.059	0.221	0.234	0.067	0.328	0.028	0.287	0.021	0.189	0.250
Ho	0.005	0.014	0.053	0.052	0.015	0.076	0.007	0.065	0.004	0.045	0.060
Er	0.013	0.046	0.162	0.151	0.050	0.223	0.025	0.189	0.012	0.137	0.170
Tm	0.002	0.008	0.024	0.025	0.008	0.036	0.005	0.029	0.002	0.023	0.030
Yb	0.015	0.061	0.161	0.167	0.060	0.242	0.038	0.200	0.019	0.163	0.200
Lu	0.003	0.012	0.030	0.025	0.011	0.039	0.008	0.034	0.005	0.029	0.030
Hf	0.000	0.000	0.000	0.000	0.000	0.000	0.000	0.000	0.000	0.000	0.100
Ta	0.009	0.005	0.014	0.021	0.007	0.015	0.003	0.032	0.046	0.006	0.030
Th	0.042	0.022	0.048	0.058	0.028	0.036	0.014	0.082	0.232	0.018	0.030
U	0.010	0.004	0.012	0.018	0.008	0.010	0.002	0.020	0.042	0.014	0.010
La/Yb	12.54	0.89	3.89	1.92	1.82	1.09	0.69	2.58	37.44	0.42	1.15

0.1325, with a large number of samples having very unradiogenic Os isotopic ratios (<0.12; Table 2). The sample YG-18 has an $^{187}Os/^{188}Os$ ratio of 0.1106, which is among the lowest values measured so far for the Chinese mantle xenoliths in Cenozoic basalts (Wu et al., 2006; Xu et al., this volume). The most refractory sample YG-19 and a LREE-enriched sample YYB-3 have $^{187}Os/^{188}Os$ higher than that of the present-day primitive

								Fansi			
YG-2	YG-5	YG-6	YG-7	YG-11	YG-12	YG-18	YG-19	FS-1	FS-2	SF-18	SF-23
44.27	44.55	44.45	44.12	44.20	44.75	42.73	38.48	45.62	44.35	44.22	44.15
0.12	0.05	0.09	0.08	0.05	0.11	0.02	0.01	0.14	0.07	0.09	0.05
3.69	1.74	2.71	2.54	1.48	3.09	1.20	0.36	4.00	1.97	2.57	2.24
9.47	9.36	9.52	8.67	9.11	8.41	9.43	11.06	9.26	8.43	8.86	9.77
38.34	43.38	39.77	40.87	44.09	39.59	46.12	50.00	36.64	42.86	39.85	40.69
0.14	0.13	0.13	0.12	0.13	0.12	0.13	0.14	0.13	0.11	0.12	0.13
3.50	0.86	2.54	2.87	0.82	3.05	0.73	0.12	3.28	1.87	3.87	2.32
0.11	<0.001	0.08	0.08	0.01	0.18	0.11	0.00	0.30	0.00	0.37	0.00
0.00	0.00	0.02	0.01	0.00	0.01	0.00	0.00	0.02	0.01	0.00	0.00
0.03	0.01	0.02	0.02	−0.01	0.03	0.03	0.01	0.06	0.01	0.07	0.02
−0.36	−0.52	−0.07	0.13	−0.30	−0.16	0.13	−0.28	0.99	0.69	0.07	0.47
99.32	99.57	99.25	99.49	99.58	99.18	100.63	99.90	100.44	100.37	100.09	99.84
0.89	0.90	0.89	0.90	0.90	0.90	0.90	0.90	0.88	0.91	0.90	0.89
15.30	8.50	13.30	12.10	8.10	13.90	7.13	3.54	13.98	10.46	13.03	12.98
473.0	168.0	419.0	368.0	157.0	445.0	73.0	65.1	584.0	295.9	352.8	210.2
58.90	27.70	63.90	59.10	26.10	51.10	20.95	4.90	59.92	37.36	40.77	40.96
2224	2300	2749	2440	2023	2536	1817	464	2329	2698	2830	2096
1004.0	1029.0	1050.0	980.0	1042.0	979.0	918.1	961.0	1005.0	863.9	847.8	950.6
103.0	77.0	105.0	100.0	91.1	83.0	153.9	175.6	126.1	131.7	134.5	106.8
2178	1784	2261	2252	1957	1663	3088	3545	2371	2763	2389	2529
24.10	10.50	29.60	18.70	13.60	18.40	4.21	3.50	11.27	22.63	15.47	12.07
43.10	37.90	47.60	43.90	35.40	36.90	41.43	44.07	36.24	28.44	30.41	45.12
3.05	1.62	2.63	2.18	1.50	2.57	1.03	0.41	5.80	1.87	3.73	3.22
0.75	0.84	1.01	0.94	0.77	0.85	0.82	0.75	0.97	0.85	0.92	0.94
0.88	0.89	1.07	0.99	0.87	0.54	1.11	0.44	1.49	0.35	1.05	0.48
7.77	5.21	11.22	20.55	8.30	10.40	4.86	4.12	42.27	23.08	80.08	5.79
3.40	0.52	2.43	2.05	0.50	2.40	0.30	0.12	3.78	2.24	2.57	1.38
2.93	1.45	4.63	4.14	1.89	4.55	0.77	1.48	6.42	10.61	5.50	1.62
0.31	0.17	0.13	0.12	0.18	0.37	0.15	0.53	0.28	0.57	0.27	0.09
1.14	0.88	0.24	0.70	0.87	1.98	1.51	3.12	20.79	4.01	2.90	1.34
0.140	0.120	0.130	0.100	0.090	0.260	0.061	0.139	1.786	0.988	2.987	0.138
0.370	0.250	0.390	0.320	0.210	0.620	0.138	0.306	6.228	3.443	7.938	0.319
0.060	0.040	0.070	0.070	0.030	0.100	0.016	0.037	0.863	0.532	0.775	0.046
0.380	0.170	0.420	0.380	0.130	0.510	0.072	0.153	3.301	2.551	2.199	0.229
0.190	0.050	0.170	0.150	0.040	0.180	0.019	0.031	0.509	0.548	0.284	0.076
0.080	0.020	0.080	0.060	0.020	0.080	0.007	0.011	0.166	0.176	0.106	0.033
0.350	0.070	0.290	0.230	0.060	0.300	0.027	0.030	0.498	0.481	0.346	0.123
0.070	0.010	0.050	0.040	0.010	0.060	0.006	0.004	0.094	0.074	0.062	0.027
0.500	0.070	0.380	0.330	0.070	0.380	0.041	0.022	0.590	0.407	0.405	0.190
0.110	0.020	0.090	0.070	0.020	0.080	0.009	0.004	0.127	0.078	0.085	0.044
0.340	0.050	0.240	0.210	0.060	0.250	0.033	0.010	0.387	0.212	0.256	0.140
0.060	0.010	0.040	0.040	0.010	0.040	0.006	0.002	0.057	0.032	0.038	0.023
0.390	0.070	0.270	0.230	0.070	0.260	0.046	0.010	0.409	0.200	0.256	0.160
0.070	0.010	0.050	0.040	0.010	0.040	0.009	0.002	0.064	0.032	0.040	0.026
0.120	0.040	0.130	0.120	0.060	0.160	0.019	0.034	0.200	0.251	0.138	0.047
0.010	0.010	0.010	0.010	0.010	0.020	0.009	0.026	0.019	0.039	0.017	0.007
0.030	0.020	0.090	0.020	0.020	0.030	0.012	0.026	0.112	0.046	0.204	0.008
0.010	0.010	0.020	0.010	0.010	0.010	0.007	0.009	0.062	0.020	0.065	0.026
0.36	1.71	0.48	0.43	1.29	1.00	1.32	13.88	4.37	4.94	11.67	0.86

upper mantle (PUM) value (0.129±1; Meisel et al., 2001). In the plot of $^{187}Os/^{188}Os$ against Al_2O_3, these two samples and another very refractory sample (YYB-1) plot off the positive correlation defined by remaining samples (Fig. 7a). All three samples show evidence for melt percolation given their high La/Yb (Table 1) and LREE-enriched pattern (Fig. 4). According to the $^{187}Os/^{188}Os$–Al correlation trend, the Os composition

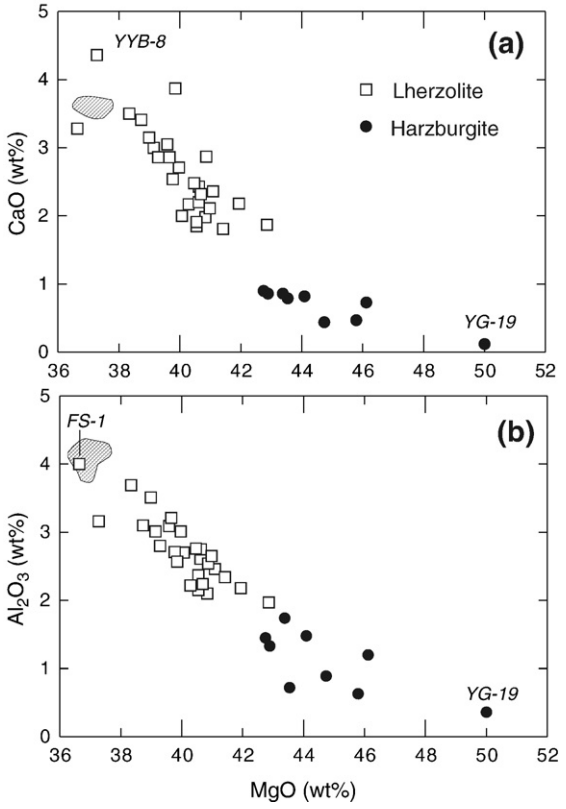

Fig. 3. Plots of CaO and Al_2O_3 against MgO for peridotite xenoliths from Yangyuan and Fansi. Diagonally hatched areas are primitive mantle compositions (Jagoutz et al., 1979; Hart and Zindler, 1986).

of the fertile lherzolite at 4.2 wt% Al_2O_3 is 0.128, which agrees well with the PUM values of Meisel et al. (2001).

5. Discussion

5.1. Depletion and enrichment events

Modal compositions (Fig. 2) reveal that the Yangyuan–Fansi peridotite xenoliths range from primitive lherzolite via clinopyroxene-poor lherzolites to strongly refractory harzburgites (Table 3). Such modal variation is accompanied by mineral and whole rock composition changes. In particular, the inverse correlations between CaO (and Al_2O_3) and MgO (Fig. 3) are similar to those observed for xenoliths from worldwide occurrences (Frey and Prinz, 1978; Xu et al., 1998; Takazawa et al., 2000). This indicates that the Yangyuan–Fansi peridotites represent the refractory residues left after extraction of the basalts by variable degrees of partial melting. Applying the method of Norman (1998), we have estimated the degrees of partial melting for the Yangyuan samples. Comparison of Y and Yb contents in lherzolite cpx and the modeled melting trend (Fig. 8) further indicates that the degrees of melting for the Yangyuan lherzolites and harzburgite varied between 0–5% and 6–20%, respectively. Nd model ages of LREE-depleted samples (2.0–2.8 Ga) suggest that melt extraction took place during Late Archean and Early Proterozoic.

LREE-enrichment associated with some moderately to highly refractory samples indicates mantle metasomatism. Chromatographic-type migration of LREE-enriched melts/fluids through LREE-depleted peridotites is an efficient metasomatic mechanism (Navon and Stolper, 1987; Bodinier et al., 1990). This type of melt-rock interaction produces REE patterns with extremely variable LREE enrichment and almost intact HREE, which is typical of that observed in the cpx studied in this paper (Fig. 4). Incipient metasomatism is associated with the samples with relatively flat REE patterns (YYB-5, 7, 8; Fig. 3c). High Nb abundance in cpx positive ε_{Nd} values and relatively low Sr/Nd and Ba/La ratios suggest that the metasomatism in these samples was probably related to small degree melts from an asthenospheric source during intraplate volcanism.

A different metasomatic agent for LREE-enriched samples (YYB-1, 3, 9) could be invoked given the strong HFSE depletion (Fig. 4e, f). Carbonatite, subduction-released fluid/melt and/or evolved asthenosphere-derived melt (Ionov et al., 1993; Bedini et al., 1997) are potential agents because they can all produce a high La/Yb and a marked HFSE depletion, as exhibited by the LREE-enriched peridotites from Yangyuan. Discrimination between these alternatives is not an easy task. However, carbonatite metasomatism is not favored given the lack of the features typical of carbonate metasomatism in the xenoliths (e.g., presence of apatite, high Na in cpx; Yaxley et al., 1998). With the exception of YYB-1, the Yangyuan samples define a roughly positive correlation between ε_{Nd} and Sm/Nd (Fig. 5b). This can be explained either by mixing between a depleted end-member and an enriched component or by time-integrated radiogenic decay.

Despite contrast in ε_{Nd} (Table 2), YYB-1 ($\varepsilon_{Nd}=+5$), YYB-3 and YYB-9 ($\varepsilon_{Nd}=-6$ to -10) have similar trace element compositions. It is thus possible that the associated metasomatic agents were likely derived from the asthenosphere by small degrees of partial melting, but metasomatism took place at a different time. The LREE enrichment associated with YYB-1 is a recent event so that the time elapsed was not sufficiently long to create low, unradiogenic $^{143}Nd/^{144}Nd$. In contrast, those associated with YYB-3 and YYB-9 must be old. The calculation suggests that the enrich-

Table 2
Trace element concentration in clinopyroxenes from Yangyuan peridotites (ppm)

	YYB-1	YYB-2	YYB-3	YYB-4	YYB-5	YYB-6	YYB-7	YYB-8	YYB-9	YYB-10	YG-1	YG-2	YG-3	YG-5	YG-6	YG-7	YG-11	YG-12
Sc	77.75	73.55	75.03	114.5	75.88	55.65	63.86	150.1	62.33	53.88	78.4	66.27	57.59	78.58	53.87	63.71	73.29	63.34
Ti	400	1086	1220	1759	1733	2738	888	2361	143	2044	2380	1775	1793	1576	1826	1974	1626	2183
V	219.5	229.1	246	272.6	231.9	238.4	230.6	294.1	150.7	223.7	295	247	205	196	195	226	202	207
Cr	8765	8319	5567	8332	6769	5718	9186	8994	5044	6451	3892	5451	5572	6792	5703	5959	7841	4517
Rb	0.558	0.13	0.164	0.573	0.069	0.063	0.091	0.267	0.156	0.198	0.12	0.07	0.33	0.07	0.1	0.13	0.21	0.13
Sr	269.8	43.6	101.1	97.22	75.48	66.39	89.02	290.8	158.7	54.53	29.13	46.47	48.6	72.48	73.67	48.07	55.6	36.13
Y	5.182	9.027	15.54	17.48	10.95	19.16	9.989	25.56	1.681	17.25	23.53	18.18	16.14	13.61	18.32	17.46	16.52	19.61
Zr	28.12	16.34	41.26	27.68	14.81	33.72	19.2	39.09	7.215	22.58	13.88	21.04	23.09	18.73	22.55	25.17	38.56	30.28
Nb	2.528	0.501	1.046	1.079	0.52	0.483	0.999	3.874	1.686	0.935	0.07	0.49	0.73	0.49	0.59	0.48	0.47	0.38
Ba	2.868	1.48	2.555	7.223	1.075	1.886	5.047	6.135	3.8	2.397	0.75	1.36	6.22	2.55	0.54	1.72	1.7	2.25
La	13.68	0.649	6.229	1.412	1.529	1.111	1.827	4.502	30.06	0.835	0.23	0.73	1.15	2.72	0.85	0.89	0.1	0.74
Ce	30.51	2.047	19.14	4.306	4.872	3.907	4.824	9.012	33.17	2.545	0.93	2.48	3.54	7.08	2.93	3.22	3.32	2.59
Pr	3.798	0.409	2.942	0.792	0.861	0.787	0.803	1.286	1.856	0.46	0.24	0.49	0.65	1.08	0.55	0.65	0.63	0.53
Nd	15.09	2.485	12.67	4.494	4.531	4.586	4.289	6.482	5.204	3.068	1.88	2.91	3.85	5.64	3.55	4.09	3.82	3.47
Sm	2.669	0.897	2.338	1.501	1.329	1.728	1.351	2.115	0.654	1.362	1.09	1.17	1.39	1.72	1.44	1.6	1.46	1.51
Eu	0.826	0.359	0.715	0.63	0.492	0.713	0.475	0.888	0.151	0.574	0.49	0.5	0.57	0.62	0.61	0.69	0.62	0.69
Gd	2.057	1.233	2.283	2.3	1.706	2.692	1.633	3.282	0.429	2.287	1.95	1.82	1.97	2	2.21	2.45	2.13	2.49
Tb	0.286	0.231	0.406	0.443	0.293	0.518	0.277	0.642	0.061	0.455	0.4	0.36	0.38	0.36	0.43	0.46	0.42	0.51
Dy	1.332	1.55	2.721	3.003	1.962	3.471	1.851	4.185	0.318	3.164	2.89	2.5	2.5	2.25	2.93	3.1	2.83	3.54
Ho	0.198	0.312	0.559	0.612	0.395	0.711	0.364	0.913	0.057	0.646	0.65	0.54	0.53	0.47	0.62	0.66	0.59	0.75
Er	0.409	0.859	1.581	1.761	1.092	1.991	1.014	2.502	0.167	1.809	1.86	1.52	1.43	1.26	1.72	1.79	1.64	2.12
Tm	0.054	0.13	0.234	0.258	0.166	0.291	0.15	0.377	0.025	0.254	0.31	0.25	0.23	0.2	0.28	0.29	0.27	0.35
Yb	0.343	0.88	1.566	1.649	1.072	1.884	0.946	2.49	0.185	1.638	1.99	1.51	1.43	1.22	1.67	1.71	1.62	2.12
Lu	0.054	0.135	0.242	0.252	0.175	0.294	0.153	0.388	0.033	0.257	0.31	0.23	0.22	0.19	0.26	0.27	0.24	0.32
Hf	0.459	0.523	0.641	1.039	0.586	1.359	0.571	1.44	0.197	0.984	0.51	0.6	0.74	0.66	0.78	0.86	1.23	0.95
Ta	0.185	0.043	0.112	0.114	0.064	0.052	0.06	0.275	0.074	0.039	0.01	0.03	0.06	0.03	0.04	0.03	0.05	0.03
Th	1.163	0.049	0.161	0.082	0.053	0.035	0.113	0.761	8.724	0.085	0.14	0.12	0.12	0.04	0.25	0.34	0.34	0.39
U	0.262	0.011	0.051	0.017	0.012	0.009	0.025	0.12	1.02	0.02	0.01	0.01	0.02	0.07	0.1	0.01	0.01	0.01
La/Yb	39.88	0.74	3.98	0.86	1.43	0.59	1.93	1.81	162.49	0.51	0.12	0.48	0.80	2.23	0.51	0.52	0.06	0.35

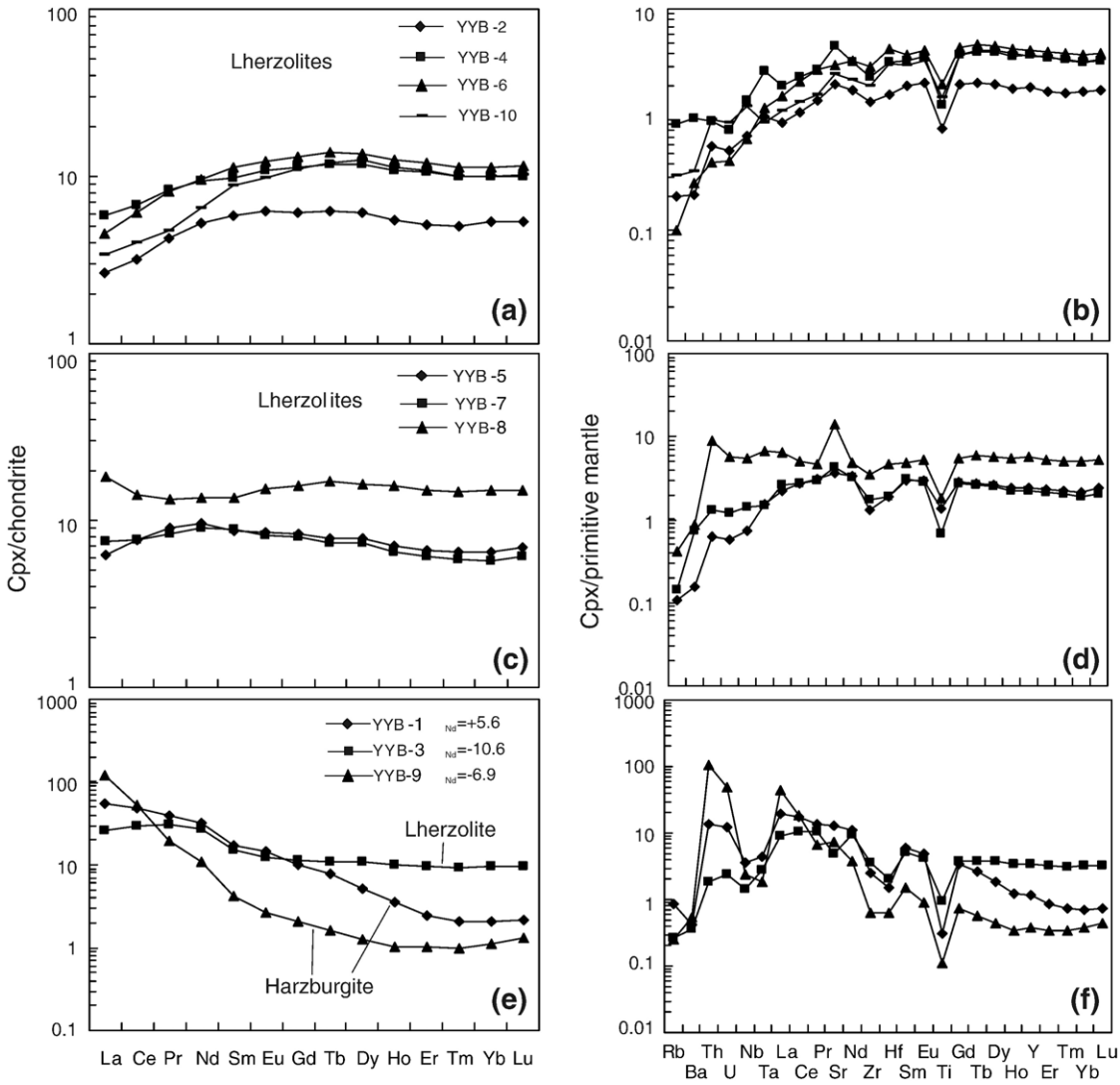

Fig. 4. REE and trace element abundances in clinopyroxenes from Yangyuan peridotites. On the left, the REE patterns normalized by chondrite values (Sun and McDonough, 1989). On the right hand are spider diagrams with trace elements normalized to primitive mantle values (Sun and McDonough, 1989).

ment must have taken place at least 1000 Ma ago so that radiogenic decay subsequent to LREE enrichment can produce low ε_{Nd} observed in these samples. A weakness of this interpretation comes from Os data. As will be discussed later, YYB-3, which is only moderately depleted in terms of Al_2O_3, likely contains a mixture of primary and secondary sulfides, whereas highly refractory YYB-1 is likely dominated by metasomatic sulfides. If both samples were metasomatized by a similar melt, then a higher $^{187}Os/^{188}Os$ ratio is expected for YYB-1 that has relatively higher Os abundances (1.6 ppb) compared to YYB-3 (~0.5 ppb). However, an opposite is observed (Table 2).

Although the problem mentioned above can be explained if the enrichment of lithophile elements and the introduction of Os took place by separated processes, a more plausible interpretation is that LREE-enriched samples with negative ε_{Nd} were affected by a metasomatic agent that is different from the asthenospheric melts invoked for the samples with positive ε_{Nd}. Subduction-related melts are the likely candidate. This suggestion is consistent with the fact that studied area is located within the Trans-North China Orogen formed as a result of collision between the western Block and eastern Block during the Early Proterozoic (Zhao et al., 2001).

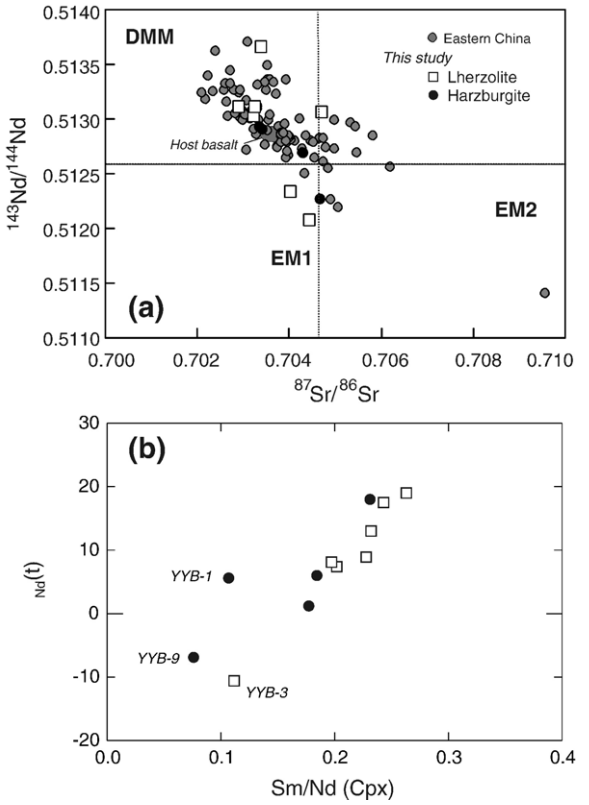

Fig. 5. (a) $^{143}Nd/^{144}Nd$ versus $^{87}Sr/^{86}Sr$ of clinopyroxene separates from the Yangyuan peridotites. Isotope data of peridotite xenoliths from eastern China (Fan et al., 2000; Song and Frey, 1989; Tatsumoto et al., 1992; Xu et al., 1998, 2003; Rudnick et al., 2004) and of the host basalts (Ma and Xu, 2004) are shown for comparison. (b) ε_{Nd} versus Sm/Nd diagram.

5.2. Effect of metasomatism on Re–Os system

A number of the Yangyuan–Fansi samples show signs of mantle metasomatism (e.g., LREE-enrichment). However, only three of them plot off the general trend in the $^{187}Os/^{188}Os$–Al plot (Fig. 7a) due to their relatively high $^{187}Os/^{188}Os$, whereas remaining metasomatized samples and unmetasomatized define a coherent correlation between $^{187}Os/^{188}Os$ and Al_2O_3. This correlation may be of age significance (see next section for age determination) or represents a mixing line reflecting refertilization of the lithosphere (Beyer et al., 2007) and/or by metasomatism of a sulfide-saturated silicate melt that introduced silicate phases (Pearson et al., 2004). However, the interpretation invoking metasomatism/refertilization is problematic for the following reasons: (a) There is no correlation between $^{187}Os/^{188}Os$ and Os for the studied samples, as would be expected with a mixing trend. Moreover, Os addition through lithospheric refertilization or metasomatism would produce a curved array (Reisberg and Lorand, 1995), rather than the linear correlation observed in Yangyuan–Fansi samples; (b) Metasomatic enrichment tends to be involved to a greater degree in more refractory samples than in more fertile samples (Frey and Prinz, 1978; Xu et al., 1998; this study), which is the opposite required to explain the positive $^{187}Os/^{188}Os$–Al_2O_3 correlation. There is no petrographic and geochemical evidence for a large-scale metasomatism that affected the whole sample suite, as the presence of LREE-depleted and high ε_{Nd} peridotites (Table 1 and Figs. 4 and 5) reflects a long-term isolation from the convecting mantle since the melting event. In fact, Al_2O_3 contents in peridotites, which are negatively correlated with MgO, are most likely controlled by depletion event. And (c) The extension of the $^{187}Os/^{188}Os$–Al_2O_3 correlation overlaps with the PUM Os isotopic composition of Meisel et al. (2001). Similar trends have been observed in peridotite xenoliths worldwide (e.g., Meisel et al., 2001; Peslier et al., 2000a; Handler et al., 2003; Wu et al., 2003, 2006; Reisberg et al., 2005) and in peridotite massifs (Reisberg and Lorand, 1995). These trends most likely resulted from radiogenic ingrowth of ^{187}Os

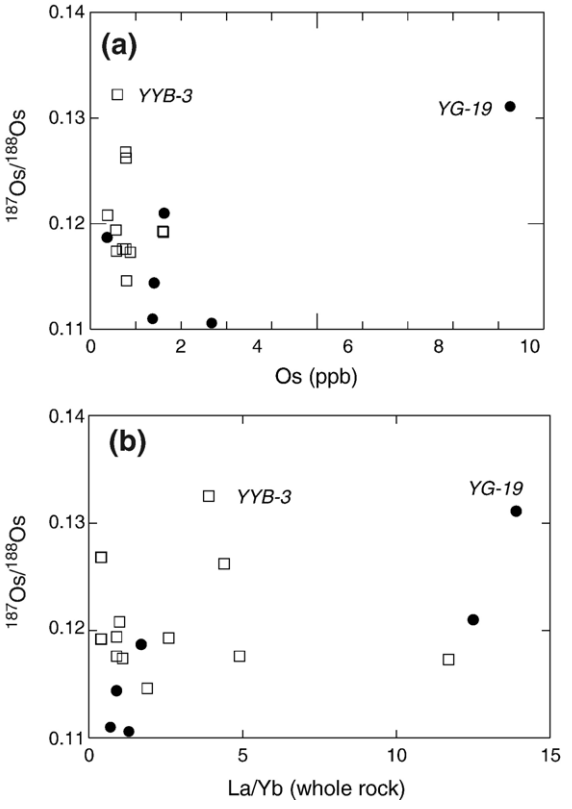

Fig. 6. $^{187}Os/^{188}Os$ versus Os and La/Yb.

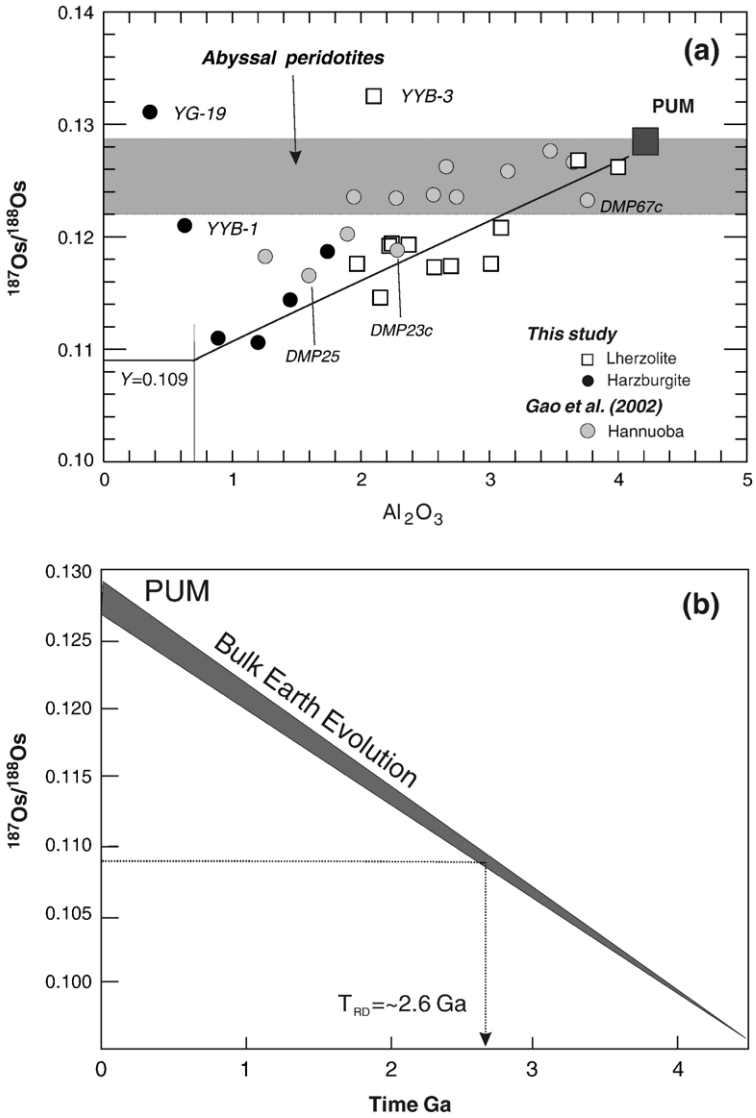

Fig. 7. (a) Whole $^{187}Os/^{188}Os$ ratios plotted against Al_2O_3 (wt%) and (b) model age determination. Os mantle evolution curve is calculated using the Os isotopic composition of the present-day PUM of Meisel et al. (2001) and initial $^{187}Os/^{188}Os$ ratio (0.09531) used by Shirey and Walker (1998). The abyssal peridotite data are from Snow and Reisberg (1995). Data for Hannuoba peridotites are from Gao et al. (2002).

subsequent to an ancient melt extraction event during which different degrees of melt extraction resulted in different degrees of Re–Os fractionation.

If the positive $^{187}Os/^{188}Os$–Al_2O_3 correlation is not a mixing line, it follows that the major Os modification affected only three samples (YYB-1, YYB-3 and YG-19) that deviate from the trend (Fig. 7a). Because of the extremely high partition coefficients for Os in sulfides, metasomatic sulfides can contain 1–10 ppm Os. Consequently, addition of metasomatic sulfides to mantle residues is an effective way to disturb both the Os abundance and Os isotopic ratios of the host peridotites. Recent investigation using the in situ techniques revealed multiple generations of sulfides in mantle peridotites. For instance, Alard et al. (2002) reported two types of sulfides in peridotite xenoliths: the "original" type was included in silicate phases and the secondary type was interstitial along silicate boundaries. Osmium abundances in interstitial sulfides are significantly lower than those of the primary sulfides (Alard et al., 2002). The whole rock analyses integrate these different generations of sulfides. Whether its Re–Os composition is affected by metasomatism depends upon the proportion between primary sulfides and secondary

Table 3
Sr–Nd–Os isotope and other data for peridotites xenoliths from Yangyuan and Fansi, western North China Craton

Sample	OL	CPX	OPX	SP	T (°C)	Al_2O_3	Mg#ol	Cr#sp	$^{87}Sr/^{86}Sr$	$^{143}Nd/^{144}Nd$	ε_{Nd}	T_{CHUR} (Ga)	$^{187}Os/^{188}Os$	Os ppt	T_{RD} (Ga)
Yangyuan															
YYB-1	81.3	1.2	16.3	3.4	1040	0.63	91.6	0.58	0.703400±15	0.512911±9	5.3	−0.5	0.1210	1624.6	1.18
YYB-2	64.5	1.8	31.4	0.9		1.45	91.8	0.31	0.703089±17				0.1124	1404.2	2.14
YYB-3	57.6	7.0	32.9	1.2	872	2.10	91.1	0.18	0.704437±15	0.512077±9	−11.0	1.0	0.1325	558.8	−0.53
YYB-4	56.9	6.4	35.0	0.8	1079	2.15	91.9	0.22	0.703234±18	0.513019±13	7.4	9.7	0.1146	797	2.11
YYB-5	66.9	2.1	29.0	0.7	832	1.33	91.0	0.23	0.704282±14	0.512694±10	1.1	−0.2			
YYB-6	58.9	7.1	31.1	1.5	1092	2.70	90.9	0.15	0.703266±11	0.513102±14	9.1	2.6	0.1174	573.1	1.71
YYB-7	71.5	0.6	25.7	0.2	1103	0.89	91.8	0.36	0.702909±14	0.513102±12	8.9	−10.8	0.1110	1369.7	2.63
YYB-8	57.8	6.7	31.6	1.2	1022	2.37	91.3	0.17	0.704708±17	0.513056±10	8.1		0.1193	1593.3	1.43
YYB-9	64.8	1.4	31.4	1.6	983	0.72	91.9	0.56	0.704710±14	0.512260±13	−7.4	0.5			
YYB-10	60.8	8.4	27.5	1.0	1113	2.22	91.4	0.19	0.703405±17	0.513658±13	19.6	2.0	0.1192	1610.9	1.45
YG-2	61.7	18.8	16.9	2.7	977	3.69				0.513498±9	17.5	2.8	0.1268	776.2	0.33
YG-5	69.2	3.6	25.3	1.7	883	1.74	90.5	0.24	0.703348±16	0.512914±6	6	−3.5	0.1187	365.9	1.52
YG-12	59.8	14.3	22.8	2.2	901	3.09	90.5	0.11		0.513595±10	19	2.2	0.1208	376	1.21
YG-18	81.9	2.5	13.6	1.6	942	1.20	90.6	0.16					0.1106	2674.1	2.69
YG-19						0.36	90.1	0.26					0.1311	9258.9	−0.31
Fansi															
FS-1	47.2	15.0	33.3	2.6	982	4.00	89.2	0.09					0.1262	783.8	0.42
FS-2					914	1.97	90.3	0.18					0.1176	709	1.68
SF-18						2.57							0.1173	879.7	1.72
SF-23	63.4	9.8	23.8	1.9	959	2.24	89.1	0.17					0.1194	563.1	1.42

Note: (1) T is calculated according to Brey and Kohler (1990). (2) Os concentration and isotopic ratios are measured by ICP-MS at WHOI. (3) The parameters used in calculation are $\lambda_{Re}=1.666\times10^{-11}$/year, $(^{187}Re/^{188}Os)_{Chod}=0.40186$, $(^{187}Os/^{188}Os)_{Chon,0}=0.129$. (4) $\lambda_{Sm}=6.54\times10^{-12}$/year, $(^{147}Sm/^{144}Nd)_{bulk\ Earth}=0.1967$, $(^{143}Nd/^{144}Nd)_{bulk\ Earth}=0.512638$.

sulfides. Specifically, the effect of such metasomatic sulfide addition on the whole rock Os isotopic systematics is only significant when the primary sulfides have been completely removed in the peridotites (Handler et al., 2003).

The fact that LREE-enriched samples (YYB-5, YYB-7, YG-5) do not display high $^{187}Os/^{188}Os$ ratio and plot along the $^{187}Os/^{188}Os$–Al correlation suggests that not all types of metasomatism can affect Re–Os isotopic system of the mantle. Such a decoupling between enrichment of lithophile and siderophile elements may be due to the relatively high proportion between primary sulfides and metasomatic sulfides in these samples. As indicated previously, these samples were affected by chromatographic metasomatism at very low melt/rock ratio. In this case, the percolating melts may be evolved thus having high concentration of LILE but low contents of siderophile elements due to sulfide segregation during precedent evolution. As a consequence, metasomatism cannot introduce a significant amount of siderophile elements, and the residual primary sulfides in these peridotites still dominate the Os budget.

YYB-3 has Os abundances (0.55 ppb) that are significantly lower than those of the other peridotites from the same locality, making it more susceptible to metasomatic Os addition. Hence, a straightforward explanation is that the high $^{187}Os/^{188}Os$ ratios in YYB-3 could have developed as a result of addition of a radiogenic Os component to the peridotites. The

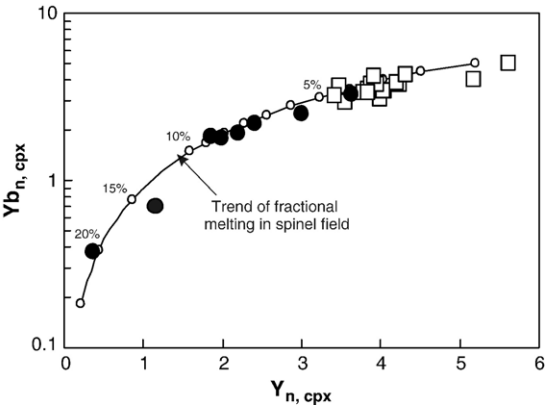

Fig. 8. Comparison of Y and Yb contents of clinopyroxenes in peridotite xenoliths from south China with the calculated melting trend using fractional melting model within spinel stability field (Norman, 1998). The subscript n in panel a indicates that the Yb and Y concentrations are normalized to primitive mantle (Sun and McDonough, 1989).

measured high $^{187}Os/^{188}Os$ reflects the mixing between primary sulfide and a metasomatic component that has more radiogenic composition. So far, radiogenic Os combined with low Os abundances has been documented in peridotite xenoliths from subduction setting (Brandon et al., 1996) and peridotites that have been modified by plume-derived melts (Handler et al., 2003). Given the Nb–Ta depletion and negative ε_{Nd} value for YYB-3, an interpretation involving supra-subduction zone processes is likely. Alternatively, high $^{187}Os/^{188}Os$ ratio was developed as a result of radiogenic ingrowth subsequent to metasomatic enrichment of Re/Os.

A similar explanation may be put forward for YYB-1, but the positive ε_{Nd} observed in this sample requires a different and recent metasomatic event. YG-19 and YYB-1 are highly refractory with Al_2O_3 of 0.36 and 0.63%, respectively. It is possible that the original Os component in these rocks may have been largely removed during melt extraction, allowing the secondary Os to dominate its current Os budget. Lithophile element compositions suggest that the metasomatic agent has a geochemical affinity with asthenospheric melts. Asthenosphere-derived melts are generally more radiogenic than most peridotites, thus accounting for the high $^{187}Os/^{188}Os$ ratios observed in these two refractory samples. The effect of radioactive decay is negligible given the recent melt infiltration processes. YG-19 has anomalously high Os concentration (>9 ppb), while the Os concentration in YYB-1 (1.6 ppb) is typical of those observed in other samples from the same localities. This may be related to the sulfide saturation of percolating melt during its passage in the lithosphere. The percolating melt associated with YG-19 probably deposited sulfides in peridotites, whereas the melts percolating YYB-1 may be relatively depleted in Os due to previous loss of sulfides.

5.3. Ages of the lithospheric mantle beneath the western NCC

The re-depletion ages (T_{RD}) for the Yangyuan samples (except for YG-19), assuming a Re/Os of zero (Walker et al., 1989), range from 0.33 to 2.69 Ga (Table 1). Because Re-contents in peridotites are certainly higher than zero after melt extraction, T_{RD} may underestimate the true ages of melting events and are considered as minimum model ages (Walker et al., 1989). Only the re-depletion age of the most refractory samples may approach that of the true age. In this sense, 2.7 Ga may represent the age of melt extraction although this is still a minimum estimate given the presence of more refractory samples.

Another method to obtain the melt-depletion age is to use Al_2O_3 as proxy of Re/Os because Al_2O_3 are positively correlated with Re/Os (e.g., Reisberg and Lorand, 1995). The $^{187}Os/^{188}Os–Al_2O_3$ correlation is interpreted as a result of radiogenic ingrowth of ^{187}Os subsequent to an ancient melt extraction event. The age of this event can be estimated by comparing the *y*-intercept of the correlation with the mantle evolution curve assuming the Re/Os of the PUM (Meisel et al., 2001). Because in refractory peridotites, Al_2O_3 contents rarely reach zero, consequently the Al-model age may overestimate the true depletion age (Pearson, 1999; Peslier et al., 2000a,b). Handler and Bennett (1999) argued that extrapolation to of 0.7 wt% is warranted because in most peridotite suites worldwide Re/Os approaches zero at that approximate level of depletion. YG-19, YYB-1 and YYB-3 are not used in model age determination because their Os isotopic compositions have been modified during melt percolation processes. The remaining samples define a positive $^{187}Os/^{188}Os–Al_2O_3$ correlation with the *y*-intercept (at Al_2O_3=0.7 wt%) at ~0.1085, yielding a model age of ~2.7 Ga (Fig. 7b). This age is in agreement with the T_{RD} of the most refractory samples and the Nd model ages of the LREE-depleted samples (2.0–2.8 Ga, Table 1), suggesting a long-term isolation of the lithospheric mantle from the convective asthenosphere. These model ages of melt extraction are virtually identical to the Nd model age of overlying crust (Wu et al., 2005), suggesting an essentially coupled crust–mantle in the western NCC.

The antiquity of the lithospheric mantle under the western NCC is also consistent with the unusual EM1 type Sr–Nd isotope composition of some LREE-enriched samples. Similar isotopic characteristics have been observed in garnet inclusion from south Africa and xenoliths and megacrysts from Outer Hebrides from Scotland, which have been interpreted as a result of radiogenic decay after a LREE-enrichment (Richardson et al., 1984; Menzies and Halliday, 1988).

5.4. Lateral variation in age structure of the upper mantle beneath the NCC

A number of Os isotope studies are now available on mantle xenoliths from eastern China, thus enabling us to gain insights into the lateral variation in the age structure of the upper mantle in this region. In the following, we compare the mantle domains across the DTGL as this lineament may represent a fundamental boundary in eastern China and its formation may be

genetically related to the lithospheric removal (Xu, 2007).

Gao et al. (2002) reported a Re–Os isochron age of 1.9 Ga for selected xenoliths from Hannuoba, which is also located to the west of the DTGL. This age is significantly younger than the Nd model age of the overlying crust, suggesting a decoupled crust and mantle at Hannuoba. These authors suggested that some portion of the original Archean lithospheric mantle underlying Hannuoba was removed during the Proterozoic, and was replaced with new lithosphere derived from the convective mantle. The decoupled crust–mantle at Hannuoba contrasts with the coupled crust–mantle at Yangyuan although the two localities are geographically proximal (Fig. 1). It is interesting to note that the majority of the Hannuoba data plot above the trend defined by the Yangyuan and Fansi peridotites (Fig. 7a). Their $^{187}Os/^{188}Os$–Al_2O_3 correlation is poorer than the $^{187}Os/^{188}Os$–Re/Os correlation (see Fig. 6b of Gao et al., 2002) and does not extend through the PUM. Since Al_2O_3 is generally less sensible to metasomatism than Re, this observation may suggest that Re–Os system has significantly been affected by metasomatic sulfide addition; specifically the $^{187}Os/^{188}Os$–Re/Os correlation observed for the Hannuoba peridotites may actually reflect a mixing between primary sulfide with unradiogenic $^{187}Os/^{188}Os$ and secondary sulfides with superchondritic $^{187}Os/^{188}Os$. Additional supporting evidences for this interpretation include (a) three samples (DMP-67c, DMP-25, DMP-23c) that are situated at the lower part for the Hannuoba array (Fig. 7c) and follow the trend defined by the Yangyuan–Fansi samples. Interestingly S abundances (20–23 ppm) in these samples are conspicuously lower than in the rest of the Hannuoba samples (mostly between 100 and 320 ppm, Gao et al., 2002). S abundances higher than 80 ppm are commonly found in peridotites that show evidence of metasomatic sulfide addition (Alard et al., 2002). (b) Recent in situ investigations suggest that metasomatic sulfides could constitute over 75% of the total sulfides in most of the peridotite samples from Hannuoba (X. Xu et al., this volume).

If the above re-evaluation is correct, the data of the least-affected samples (i.e., DMP-67c, DMP-25 and DMP-23c) can be used to back-up the timing of melt extraction events in the Hannuoba area. They define an $^{187}Os/^{188}Os$–Al_2O_3 correlation that is similar to that for the Yangyuan–Fansi samples (Fig. 7b), suggesting that the mantle xenoliths from western NCC record the same stabilization age (i.e., Late Archean to very Early Proterozoic). The assessment of the Early Proterozoic mantle at Yangyuan, Fansi and Hannuoba suggests that fertile mantle can persist for a prolonged time (Lee et al., 2001). The contrast in composition between Archean and Proterozoic mantle implies a dramatic change in thermal condition from the Archean to the Proterozoic (Menzies, 1990; Griffin et al., 1998).

A complex age structure is found for the lithospheric mantle beneath the eastern NCC. For instance, some highly refractory samples from Longgang (Jilin Province) and Qixia (Shandong Province) have T_{RD} age of 1–1.2 Ga, suggesting a minimum Mesoproterozoic model age for melt depletion of the SCLM underlying some portions of the eastern NCC (Gao et al., 2002; Wu et al., 2003). Reisberg et al. (2005) reported Re–Os isotopic data on peridotite xenoliths from Subei basin (east Central China) and suggested the mantle underneath this region were affected by an Early Proterozoic (~1.8 Ga) melt extraction event. More recently, Wu et al. (2006) obtained a model age of ~2.3 Ga for Kuandian peridotites. All these data point to the presence of ancient mantle residues in the eastern NCC. On the other hand, a number of samples from the eastern NCC show Os isotopic data overlapping that of the modern convecting upper mantle defined by abyssal peridotites and ophiolites, and their T_{RD} ages range from 0.4 to 0 Ga (Gao et al., 2002; Wu et al., 2003). This may indicate the presence of much younger portion of the lithospheric mantle. It is possible that the upper mantle beneath the eastern NCC comprises both ancient melting residues and newly accreted material (e.g., Gao et al., 2002; Wu et al., 2003, 2006), although their spatial resolution is unclear.

The Os model ages for the upper mantle from the eastern NCC are significantly younger than the formation age of the overlying crust (Wu et al., 2005), suggesting a decoupled crust–mantle system in this region. This contrasts with the coupled crust–mantle system in the western NCC, thereby outlining the lateral heterogeneity of the lithospheric mantle beneath the NCC. This is consistent with the view that lithospheric removal was largely limited to the eastern NCC. The different lithospheric structure in the western and eastern NCC could be due to the diachronous extension history that resulted from interaction of two tectonic regimes (Xu et al., 2004b). While the extension in the Shanxi graben was likely related to the Indo-Eurasian collision (Ye et al., 1987), the NNE-trending basins in the eastern NCC may be induced by subduction of the Pacific plate underneath the Asian continent (Griffin et al., 1998; Wu et al., 2003; Xu et al., 2004b), which started probably since the end of the Mesozoic (Engebretson

et al., 1985). On the other hand, the co-existence of new and old mantle in the eastern NCC is not consistent with the delamination model in which the removal of the entire old mantle is expected (Reisberg et al., 2005).

Available Os isotopic data point to the presence of Archean mantle residues prior to the lithospheric thinning (Gao et al., 2002; Wu et al., 2006). If the thermal erosion model applies, the co-existence of Archean relicts and new mantle components is expected. However, Cenozoic basalts essentially sampled both Proterozoic mantle and newly accreted mantle with $^{187}Os/^{188}Os$ consistent with those of modern convecting mantle (Gao et al., 2002; Wu et al., 2003, 2006). A key issue needs to be addressed is why there is no sign of Archean mantle under the eastern NCC. One possibility is that Archean sulfides are masked by whole-rock analyses if post-Archean sulfide metasomatism is significant. However, the fertile nature of the peridotites hosted in Cenozoic basalts renders the Archean age for the formation of the lithosphere under eastern China unlikely. Three additional alternatives have recently been conceived by Wu et al. (2006), including inverted age stratigraphy in the lithospheric mantle during the Paleozoic, preferential sampling of Proterozoic and modern age mantle by Cenozoic volcanism and replacement of Archean mantle during thinning by Proterozoic–Phanerozoic mantle that formed underneath the Yangtze craton. Testing of these models requires information about the spatial variation in the age structure of the lithosphere prior to thinning. This is, however, hampered by limited and geographically restricted occurrences of pre-Mesozoic, xenolith-bearing volcanism. Nevertheless, the "exotic" Proterozoic mantle as implied by the third alternative is not consistent with the accumulating evidence for an intense and widespread Paleoproterozoic mantle melting event in the eastern NCC. For instance, the granulite xenoliths in the Fuxian kimberlites were formed at 2.5 Ga and represent underplates ($\varepsilon_{Hf}(t)$=2.4–8.4) of a significant magmatic event (Zheng et al., 2004). Similar 2.5-Ga zircons with positive Hf composition are preserved in the Mesozoic intrusions in Shandong province (Xu et al., 2007), suggesting that the Proterozoic mantle is indeed an intrinsic component of the lithospheric mantle under the eastern NCC. It is likely that the upper mantle prior to the lithospheric thinning was composed of both Archean and Proterozoic residues, although the spatial relation of these two components is unclear yet. The Phanerozoic mantle may have formed as a result of conductive cooling of upwelled asthenosphere that emplaced at the space left by the thinning of pre-existing lithospheric keel (Xu, 2001).

6. Conclusions

(1) The lithospheric mantle sampled by the Yangyuan and Fansi Cenozoic volcanism (western NCC) is chemically and isotopically heterogeneous. Parts of the lithospheric mantle are characterized by moderately to strongly refractory mantle with variable enrichment in LILE. The Yangyuan samples show a wide range in Sr–Nd isotopic composition from DMM to EM-1-like component. The lithospheric mantle beneath the western NCC experienced multiple metasomatic enrichments involving small melt fractions derived from the asthenosphere and melts related to a supra-subduction setting.

(2) The Yangyuan–Fansi peridotites are characterized by a wide range in Os isotopic ratio (0.110–0.133). The unradiogenic Os isotopic ratios in some refractory samples provide evidence for the existence of ancient lithosphere under the western NCC. Correlations between $^{187}Os/^{188}Os$ and Al_2O_3 yield a model age of ~2.6 Ga, suggesting that the lithospheric mantle beneath the western NCC was stabilized in the Late Archean or very Early Proterozoic. This model age overlaps the Nd modal age of overlying crust, reflecting a coupled crust–mantle beneath the western NCC.

(3) The coupled crust–mantle in the western NCC contrasts with the decoupled nature in the eastern NCC. This confirms that the notion that the lithospheric removal was largely limited to the eastern NCC. The co-existence of new and old mantle in the eastern NCC is not consistent with the delamination model in which the removal of the entire old mantle is expected. The different lithospheric structure in the western and eastern NCC could be due to the diachronous extension history that resulted from interaction of the Pacific subduction-controlled regime and Indo-Euroasian collision regimes.

Acknowledgments

We thank Richard Walker, Fuyuan Wu and an anonymous referee for constructive comments that help improve the quality of the paper. The authors gratefully acknowledge the financial support from the National Science Foundation of China (40673038; 49925308), the Chinese Academy of Sciences and China Scholarship Council to YGX for a six-month visit to the USA and from Japan Society for the Promotion of Science to KS (Grant-in Aid #14703002).

References

Alard, O., Griffin, W.L., Pearson, N., Lorand, J.P., O'Reilly, S.Y., 2002. New insights into the Re–Os systematics of sub-continental lithospheric mantle from in-situ analyses of sulfides. Earth Planet. Sci. Lett. 203, 651–663.

Bedini, R.M., Bodinier, J.-L., Dautria, J.M., Morten, L., 1997. Evolution of LILE-enriched small melt fractions in the lithospheric mantle: a case study from the East Africa Rift. Earth Planet. Sci. Lett. 153, 67–83.

Beyer, E.E., Griffin, W.L., O'Reilly, S.Y., 2007. Transformation of archaean lithospheric mantle by refertilization: evidence from exposed peridotites in the Western Gneiss region, Norway. J. Petrol. 47, 1611–1636.

Bodinier, J.-L., Vasseur, G., Vernieres, J., Dupuy, C., Fabries, J., 1990. Mechanisms of mantle metasomatism: geochemical evidence from the Lherz orogenic peridotite. J. Petrol. 31, 597–628.

Brandon, A.D., Creaser, R.A., Shirey, S.B., Carlson, R.W., 1996. Osmium recycling in subduction zones. Science 272, 861–864.

Brey, G.P., Kohler, T., 1990. Geothermobarometry in four-phase lherzolites II. New thermobarometers, and practical assessment of existing thermobarometers. J. Petrol. 31, 1353–1378.

Carlson, R.W., Irving, A.J., 1994. Depletion and enrichment history of subcontinental lithospheric mantle: an Os, Sr, Nd and Pb isotopic study of ultramafic xenoliths from the northwestern Wyoming Craton. Earth Planet. Sci. Lett. 126, 457–472.

Chesley, J., Righter, K., Ruiz, J., 2004. Large-scale mantle metasomatism: a Re–Os perspective. Earth Planet. Sci. Lett. 219, 49–60.

Engebretson, D.C., Cox, A., Gordon, R.G., 1985. Relative motions between oceanic and continental plates in the Pacific basins. Geol. Soc. Am. Spec. Paper 206, 1–59.

Fan, W.M., Zhang, H.F., Baker, J., Javis, K.E., Mason, P.R.D., Menzies, M.A., 2000. On and off the North China craton: where is the Archaean keel? J. Petrol. 41, 933–950.

Frey, F.A., Prinz, M., 1978. Ultramafic inclusions from San Carlos, Arizona: petrologic and geochemical data bearing on their petrogenesis. Earth Planet. Sci. Lett. 38, 129–176.

Gao, S., Rudnick, R.L., Carlson, R.W., McDonough, W.F., Liu, Y.-S., 2002. Re–Os evidence for replacement of ancient mantle lithosphere beneath the North China Craton. Earth Planet. Sci. Lett. 198, 307–322.

Gao, S., Rudnick, R.L., Yuan, H.-L., Liu, X.-M., Liu, Y.-S., Xu, W.-L., Ling, W.-L., Ayers, J., 2004. Recycling lower continental crust in the North China Craton. Nature 432, 892–897.

Goto, A., Tatsumi, Y., 1996. Quantitative analyses of rock samples by an X-ray fluorescence spectrometer (II). Rigaku J. 13, 20–39.

Griffin, W.L., Zhang, A.D., O'Reilly, S.Y., Ryan, G., 1998. Phanerozoic evolution of the lithosphere beneath the Sino-Korean Craton. In: Flower, M., Chung, L., Lo, H., Lee, T.Y. (Eds.), Mantle Dynamics and Plate Interactions in East Asia. Am. Geophys. Union, pp. 107–126.

Griffin, W.L., Graham, S., O'Reilly, S.Y., Pearson, N.J., 2004. Lithosphere evolution beneath the Kaapvaal Craton. Re–Os systematics of sulfides in mantle-derived peridotites. Chem. Geol. 208, 89–118.

Handler, M.R., Bennett, V.C., 1999. Behaviour of platinum-group elements in the subcontinental mantle of eastern Australia during variable metasomatism and melt depletion. Geochim. Cosmochim. Acta 63, 3597–3618.

Handler, M.R., Bennett, V.C., Esat, T.M., 1997. The persistence of off-cratonic lithospheric mantle: Os isotopic systematics of variably metasomatised southeast Australian xenoliths. Earth Planet. Sci. Lett. 151, 61–75.

Handler, M.R., Wysoczanski, R.J., Gamble, J.A., 2003. Proterozoic lithosphere in Marie Byrd Land, West Antarctica: Re–Os systematics of spinel peridotite xenoliths. Chem. Geol. 196, 131–145.

Hart, S.R., Zindler, A., 1986. In search of a bulk Earth composition. Chem. Geol. 57, 247–267.

Hassler, D.R., Peucker-Ehrenbrink, B., Ravizza, G.E., 2000. Rapid determination of Os isotopic composition by sparging OsO_4 into a magnetic-sector ICP-MS. Chem. Geol. 166, 1–14.

Ionov, D.A., Dupuy, C., O'Reilly, S.Y., Kopylova, M.G., Genshaft, Y.S., 1993. Carbonated peridotite xenoliths from Spitsbergen: implications for trace element signature of mantle carbonate metasomatism. Earth Planet. Sci. Lett. 119, 283–297.

Jagoutz, E., Palme, H., Baddenhausen, H., Blum, K., Cendales, M., Drebus, G., Spettel, B., Wanke, LorenzV., 1979. The abundances of major, minor and trace elements in the earth's mantle as derived from primitive ultramafic nodules. Proc. Lunar Planet. Sci Conf. 10th 1031–2050.

Lee, C.-T., Yin, Q.-Z., Rudnick, R.L., Jacobsen, S.B., 2001. Preservation of ancient and fertile lithospheric mantle beneath the southwestern United States. Nature 411, 69–73.

Liu, R.X., Chen, W.J., Sun, J.Z., Li, D.M., 1992. The K-Ar age and tectonic environment of Cenozoic volcanic rock in China. In: Liu, R.X. (Ed.), The Age and Geochemistry of Cenozoic Volcanic Rock in China. Seismologic Press, Beijing, pp. 1–43. In Chinese.

Ma, J.L., Xu, Y.G., 2004. Petrology and geochemistry of the Cenozoic Basalts from Yangyuan of Hebei Province and Datong of Shanxi Province: implications for the deep process in the Western North China Craton. Geochimica 33, 75–88.

Ma, X. (Ed.), 1989. Atlas of Active Faults in China. Seismological Press, Beijing, p. 120.

Meisel, T., Walker, R.J., Irving, A.J., Lorand, J.-P., 2001. Osmium isotopic compositions of mantle xenoliths: a global perspective. Geochim. Cosmochim. Acta 65, 1311–1323.

Menzies, M.A., 1990. Archean, Proterozoic, and Phanerozoic lithospheres. In: Menzies, M.A. (Ed.), Continental Mantle. Oxford Science Publications, pp. 67–86.

Menzies, M.A., Halliday, A., 1988. Lithospheric mantle domains beneath the Archean and Proterozoic crust of Scotland. J. Petrol. 275–302 (Special Lithosphere Issue).

Menzies, M.A., Xu, Y.G., 1998. Geodynamics of the North China Craton. In: Flower, M., Chung, S.L., Lo, C.H., Lee, T.Y. (Eds.), Mantle Dynamics and Plate Interactions in East Asia. Am. Geophys. Union, vol. 27, pp. 155–165.

Menzies, M.A., Fan, W.M., Zhang, M., 1993. Palaeozoic and Cenozoic lithoprobes and the loss of >120 km of Archaean lithosphere, Sino-Korean craton, China. In: Prichard, H.M., Alabaster, T., Harris, N.B.W., Neary, V.R. (Eds.), Magmatic Processes and Plate Tectonics. Geol. Soc. Spel. Pub., vol. 76, pp. 71–78.

Mercier, J.-C.C., Nicolas, A., 1975. Textures and fabrics of upper mantle peridotites as illustrated by xenoliths from basalts. J. Petrol. 16, 454–487.

Navon, O., Stolper, E., 1987. Geochemical consequence of melt percolation: the upper mantle as a chromatographic column. J. Geol. 95, 285–307.

Norman, M.D., 1998. Melting and metasomatism in the continental lithosphere: laser ablation ICPMS analysis of minerals in spinel lherzolites from eastern Australia. Contrib. Mineral. Petrol. 130, 240–255.

Pearson, D.G., 1999. The age of continental roots. Lithos 48, 171–194.

Pearson, D.G., Shirey, S.B., Carlson, R.W., Boyd, F.R., Nixon, P.H., 1995. Stabilisation of Archean lithospheric mantle: a Re–Os

isotope study of peridotite xenoliths from the Kaapvaal craton. Earth Planet. Sci. Lett. 134, 341–357.

Pearson, D.G., Irvine, G.J., Ionov, D.A., Boyd, F.R., Dreibus, G.E., 2004. Re–Os isotope systematics and platinum element fractionation during mantle melt extraction: a study of massif and xenolith peridotite suites. Chem. Geol. 208, 29–59.

Peslier, A.H., Reisberg, L., Ludden, J., Francis, D., 2000a. Os isotopic systematics in mantle xenoliths; age constraints on the Canadian Cordillera lithosphere. Chem. Geol. 166, 85–101.

Peslier, A.H., Reisberg, L., Ludden, J., Francis, D., 2000b. Re–Os constraints on harzburgite and lherzolite formation in the lithospheric mantle: a study of northern Canadian Cordillera xenoliths. Geochim. Cosmochim. Acta 64, 3061–3071.

Reisberg, L.C., Lorand, J.P., 1995. Longevity of sub-continental mantle lithosphere from osmium isotopic systematics in orogenic peridotite massifs. Nature 376, 159–162.

Reisberg, L., Zhi, X.C., Lorand, J.P., 2005. Re–Os and S systematics of spinel peridotite xenoliths from east central China: evidence for contrasting effects of melt percolation. Earth Planet. Sci. Lett. 239, 286–308.

Richardson, S.H., Gurney, J.J., Erlank, A.J., Harris, J.W., 1984. Origin of diamonds in old enriched mantle. Nature 310, 198–202.

Rudnick, R.L., Gao, S., Ling, W.L., Liu, Y.S., McDonough, W.F., 2004. Petrology and geochemistry of spinel peridotite xenoliths from Hannuoba and Qixia, North China craton. Lithos 77, 609–637.

Shirey, S.B., Walker, R.J., 1998. The Re–Os isotope system in cosmochemistry and high-temperature geochemistry. Annu. Rev. Earth Planet. Sci. 26, 423–500.

Snow, J.E., Reisberg, L., 1995. Os isotopic systematics of the MORB mantle: results from altered abyssal peridotites. Earth Planet. Sci. Lett. 136, 723–733.

Song, Y., Frey, F.A., 1989. Geochemistry of peridotite xenoliths in basalt from Hannuoba, eastern China: implications for subcontinental mantle heterogeneity. Geochim. Cosmochim. Acta 53, 97–113.

Sun, S.-S., McDonough, W.F., 1989. Chemical and isotopic systematics of oceanic basalts: implications for mantle composition and processes. In: Saunders, A.D., Norry, M.J. (Eds.), Magmatism in the Ocean Basins. Geol. Soc. Spel. Pub., vol. 42, pp. 313–345.

Takazawa, E., Frey, F.A., Shimizu, N., Obata, M., 2000. Whole rock compositional variation in an upper mantle peridotite (Horoman, Hokkaido, Japan): are they consistent with a partial melting process? Geochim. Cosmochim. Acta 64, 695–716.

Tanaka, T., Togashi, S., Kamioka, H., et al., 2000. JNdi-1: a neodymium isotopic reference in consistency with La Jolla neodymium. Chem. Geol. 168, 279–281.

Tatsumoto, M., Basu, A.R., Huang, W.K., Wang, J.W., Xie, G.H., 1992. Sr, Nd, and Pb isotopes of ultramafic xenoliths in volcanic rocks of Eastern China: enriched components EMI and EMII in subcontinental lithosphere. Earth Planet. Sci. Lett. 113, 107–128.

Walker, R.J., Carlson, R.W., Shirey, S.B., Boyd, F.R., 1989. Os, Sr, Nd, and Pb isotope systematics of southern African peridotite xenoliths: implications for the chemical evolution of subcontinental mantle. Geochim. Cosmochim. Acta 53, 1583–1595.

Widom, E., Kepezhinskas, P., Defant, M., 2003. The nature of metasomatism in the sub-arc mantle wedge: evidence from Re–Os isotopes in Kamchatka peridotite xenoliths. Chem. Geol. 196, 283–306.

Wu, F.-Y., Walker, R.J., Ren, X.-w., Sun, D.-y., Zhou, X.H., 2003. Osmium isotopic constraints on the age of lithospheric mantle beneath northeastern China. Chem. Geol. 196, 107–129.

Wu, F.-Y., Zhao, G.-C., Wilde, S.A., Sun, D.-Y., 2005. Nd isotopic constraints on the crustal formation of the North China Craton. J. Asian Earth Sci. 24, 523–545.

Wu, F.Y, . Walker, R.J., Yang, Y.H., Yuan, H.L., Yang, J.-H., 2006. The chemical–temporal evolution of lithospheric mantle underlying the North China Craton. Geochim. Cosmochim. Acta 70, 5013–5034.

Xu, Y.G, 2001. Thermo-tectonic destruction of the Archaean lithospheric keel beneath eastern China: evidence, timing and mechanism. Phys. Chem. Earth, A 26, 747–757.

Xu, Y.G., 2002. Evidence for crustal components in mantle source and constraints on recycling mechanism: pyroxenite xenoliths from Hannuoba. North China Chem. Geol. 182, 301–322.

Xu, Y.G., 2007. Diachronous lithospheric thinning of the North China Craton and formation of the Daxinganling-Taihangshan gravity lineament. Lithos 96, 281–298.

Xu, Y.G., Menzies, M.A., Vroon, P., Mercier, J.-C., Lin, C.Y., 1998. Texture–temperature–geochemistry relationships in the upper mantle as revealed from spinel peridotite xenoliths from Wangqing, NE China. J. Petrol. 39, 469–493.

Xu, Y.G., Menzies, M.A., Thirlwall, M.F., Huang, X.L., Liu, Y., Chen, X.M., 2003. "Reactive" harzburgites from Huinan, NE China: products of lithosphere-asthenosphere interaction during lithospheric thinning? Geochim. Cosmochim. Acta 67, 487–505.

Xu, Y.-G., Huang, X.L., Ma, J.L., Wang, Y.B., Iizuka, Y., Xu, J.F., Wang, Q., Wu, X.Y., 2004a. Crustal–mantle interaction during the thermo-tectonic reactivation of the North China Craton: SHRIMP zircon U-Pb age, petrology and geochemistry of Mesozoic plutons in western Shandong. Contrib. Mineral. Petrol. 147, 750–767.

Xu, Y.-G., Chung, S.-L., Ma, J., Shi, L., 2004b. Contrasting Cenozoic lithospheric evolution and architecture in western and eastern Sino-Korean Craton: constraints from geochemistry of basalts and mantle xenoliths. J. Geol. 112, 593–605.

Xu, Y.G., Wu, X.Y., Luo, Z.Y., Ma, J.L., Huang, X.L., Xie, L.W., 2007. Zircon Hf isotope compositions of Jurassic-Early Cretaceous intrusions in Shandong Province and its implications. Acta Petrol. Sin. 23, 307–316.

Yaxley, G.M., Green, D.H., Kamenetsky, V., 1998. Carbonatite metasomatism in the southeastern Australian lithosphere. J. Petrol. 39, 1917–1930.

Ye, H., Zhang, B., Mao, F., 1987. The Cenozoic tectonic evolution of the Great North China: two types of rifting and crustal necking in the Great North China and their tectonic implications. Tectonophysics 133, 217–227.

Yuan, X., 1996. Velocity structure of the Qinling lithosphere and mushroom cloud model. Sci. China, Ser. D 39, 235–244.

Zhao, G.C., Wilde, S.A., Cawood, P.A., Sun, M., 2001. Archean Blocks and their boundaries in the North China craton: lithological, geochemical, structural and P-T path constraints and tectonic evolution. Precambrian Res. 107, 45–73.

Zheng, J.P., Griffin, W.L., O'Reilly, S.Y., et al., 2004. U–Pb and Hf-isotope analysis of zircons in mafic xenoliths from Fuxian kimberlites: evolution of the lower crust beneath the North China Craton. Contrib. Mineral. Petrol. 148, 79–103.